Materials Science and Engineering B 172 (2010) 146–150

Contents lists available at ScienceDirect

Materials Science and Engineering B

journal homepage: www.elsevier.com/locate/mseb

Critical length and giant magnetoimpedance in $Co_{69}Fe_{4.5}Ni_{1.5}Si_{10}B_{15}$ amorphous ribbons

Anurag Chaturvedi[a], Tara P. Dhakal[a], Sarath Witanachchi[a], Anh-Tuan Le[b], Manh-Huong Phan[a,*], Hariharan Srikanth[a]

[a] Department of Physics, University of South Florida, Tampa, FL 33620, USA
[b] Hanoi Advanced School of Science and Technology (HAST), Hanoi University of Technology, 01 Dai Co Viet street, Hanoi, Viet Nam

ARTICLE INFO

Article history:
Received 26 January 2010
Received in revised form 26 April 2010
Accepted 28 April 2010

Keywords:
Amorphous ribbons
Length effect
Magnetoimpedance
Magnetic sensors

ABSTRACT

We report a systematic study of the influence of sample length on the giant magnetoimpedance (GMI) effect and its field sensitivity (η) in $Co_{69}Fe_{4.5}Ni_{1.5}Si_{10}B_{15}$ amorphous ribbons in the frequency range of 0.1–10 MHz. We show that there exists a critical length ($L_0 \sim 8$ mm) below which the maximum GMI and η decrease with decreasing sample length (L) and above which they increase with decreasing L. The critical frequency, at which the maximum GMI and η are achieved, reaches the largest value for samples with $L = L_0$ and shifts to lower values for samples with $L < L_0$ and $L > L_0$. Our observations provide important practical guidance for optimization of the geometrical dimensions of magnetic sensing elements and design of GMI-based magnetic sensors. The demagnetization contribution for $L < L_0$ and the origin of the existence of L_0 and f_0 are discussed in the context of the permeability and resistance dependences of GMI.

1. Introduction

Research on soft ferromagnetic materials exhibiting giant magnetoimpedance (GMI) effect for high-performance magnetic sensors is an area of topical interest [1]. The GMI effect is defined as the large change of the ac impedance of a magnetic material when a dc magnetic field is applied. GMI has been observed in a variety of materials, such as magnetic wires [2], ribbons [3] and thin films [4], and it strongly depends on the geometrical dimensions of the samples [5–10]. However, for practical applications that require fabrication of sensors of different dimensions, the sample length (L) dependence of GMI in different types of samples needs further investigation. Vazquez et al. [11] reported that the GMI effect decreased in Fe-based nanocrystalline wires as the wire length decreased from 8 to 1 cm. A similar trend was also observed for the case of Co-based amorphous ribbons [12–14], Fe-based nanocrystalline ribbons [15,16] and CoSiB/Cu/CoSiB layered thin films [5]. However, Phan et al. [17] reported that the decrease of length of a Co-based microwire from 4 to 1 mm resulted in a strong increase of the GMI effect. These varied observations lead to a general expectation that for each type of material there exists a critical length (L_0), below which the GMI effect decreases with decreasing sample length [11–15] and above which it increases with decrease of sample length [17]. This hypothesis has been supported by the previous observation of the effect of L_0 on the magnetization process in Co-based and Fe-based amorphous wires [18]. It has been shown that the spontaneous magnetic bistability of these wires is lost when the sample length becomes less than the critical length ($L < L_0$). In this case, the authors have attributed the loss of magnetic bistability to the influence of shape anisotropy, where for short wires the demagnetizing field became large enough to overcome the original domain structure of the sample [18]. Such modification in the domain structure near the extremities of the sample can result in variation in GMI features with respect to change in sample length. The decrease of GMI with decreasing L for the cases of Fe-based nanocrystalline wires [11] and Co-based amorphous ribbons [12–14] can be attributed to the formation of closure domain structures due to the demagnetization effect, when the measured sample length is less than the critical length, $L < L_0$. On the other hand, the increase of GMI effect with decreasing L for the case of Co-based microwires reported by Phan et al. [17] can be reconciled with the fact that the measured sample length is larger than the critical length, $L > L_0$. For practical applications in sensors and actuators based on GMI effect, there is an emerging need for a clear understanding of the sample length dependence of GMI in a single material.

We present here a comprehensive study of the influence of sample length ($L = 2$, 5, 8, and 10 mm) on the GMI effect and

* Corresponding author. Tel.: +1 813 974 4714.
E-mail addresses: tuanla-hast@mail.hut.edu.vn (A.-T. Le), phanm@usf.edu (M.-H. Phan), sharihar@usf.edu (H. Srikanth).

0921-5107/$ – see front matter © 2010 Elsevier B.V. All rights reserved.
doi:10.1016/j.mseb.2010.04.038

magnetic sensitivity parameter (η) (to be defined in the next section) in $Co_{69}Fe_{4.5}Ni_{1.5}Si_{10}B_{15}$ amorphous ribbons over a frequency range of 0.1–10 MHz. Our studies show that there exists a critical length ($L_0 \sim 8$ mm) in the $Co_{69}Fe_{4.5}Ni_{1.5}Si_{10}B_{15}$ amorphous ribbons, for which the largest GMI and η are achieved. Below the critical length ($L < L_0$), the GMI and η decrease with decreasing L, resulting from the possible formation of closure domain structures near the ends of the sample governed by the demagnetization effect. Above the critical length ($L > L_0$), the increase of GMI effect and η with decreasing L can be attributed to the decrease of electrical resistance. We also find that the critical frequency (f_0), at which the maximum GMI and η are achieved, reaches the largest value for samples with $L = L_0$ and shifts to lower values for samples with $L < L_0$ and $L > L_0$. These findings point to the importance of the geometrical dimensions of samples and provide some insights for optimizing the GMI effect in highly sensitive GMI-based magnetic sensors.

2. Experimental

Amorphous $Co_{69}Fe_{4.5}Ni_{1.5}Si_{10}B_{15}$ ribbons with a width of 1 mm and a thickness of 16 μm were prepared by the melt-spinning method. In this technique, the purity elements were firstly put in a quartz crucible, evacuated to a high vacuum state, then filled the crucible with highly purified argon and melted them at appropriate temperature in 5 min. The obtained ingots with a certain composition were then put into a quartz tube orifice and melted by heated high frequency induction coils wound around the tube. The jet located distance from the surface of cooling copper drum ~0.3 mm with a sloping angle $\theta \sim 1$–2°. Under pressure (~0.2 MPa), a jet of the molten alloy was injected from the orifice into the surface of a cooling copper wheel, which was rotating at a longitudinal speed of 30 m s^{-1} in Ar. The width and thickness of amorphous ribbon was controlled by tuning the dimensions of the orifice, the drum velocity, and the injection pressure. The amorphous nature of the as-quenched ribbons was examined by X-ray diffraction (XRD) and the atomic percentages of the elements were established by inductive coupled plasma spectroscopy [19]. The surface topography of the ribbon sample was analyzed using a Digital Instruments Dimension 3100 Atomic Force Microscope. The ribbon samples of different lengths of $L = 2$, 5, 8 and 10 mm were used for the present study. These samples were from the same ribbon length. Field dependent magnetization (M–H) measurements were performed at room temperature using a Physical Property Measurement System (PPMS) from Quantum Design. In these measurements, the dc magnetic field was applied parallel to the ribbon plane and in the longitudinal direction of the ribbon. Magnetoimpedance measurements were carried out along the ribbon axis in applied dc magnetic fields up to 120 Oe over a frequency range of 0.1–10 MHz with the ac current directed along the ribbon axis. The Helmholtz coil (diameter, 30 cm) produced the dc magnetic field (H_{dc}) that is perpendicular to the ac magnetic field (H_{ac}) generated by the applied ac current. The Helmholtz coil was designed and fabricated in-house and was calibrated for the field produced against the applied current. A power supply (Kepco Instruments) was used to source the dc current in the Helmholtz coil to generate the desired magnetic field. An impedance analyzer (HP4192A) was used in the four-terminal contact mode to measure the absolute value of the impedance (Z) of the sample at room temperature. A low-noise, shielded accessory test lead (Agilent 16048G) was used to connect the sample to the impedance analyzer. All the electronic instruments were controlled using LabView. A schematic diagram of the magnetoimpedance measurement system is described in Fig. 1.

From the measured impedance, the percentage change of magnetoimpedance (i.e., the GMI ratio) with applied magnetic field is

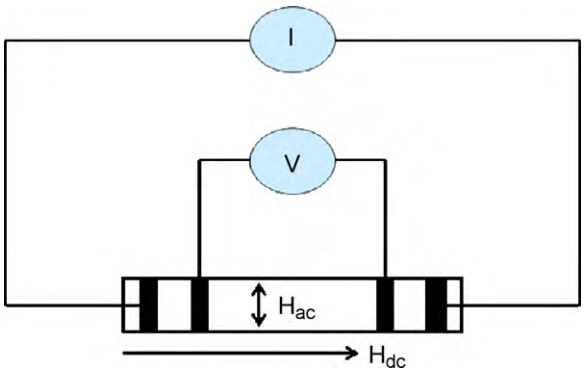

Fig. 1. Schematic view of the experimental method for measuring GMI.

expressed as

$$\frac{\Delta Z}{Z}(\%) = 100\% \times \frac{Z(H) - Z(H_{max})}{Z(H_{max})} \quad (1)$$

, and the dc magnetic field sensitivity of GMI as

$$\eta = 2 \times \frac{[\Delta Z/Z(\%)]_{max}}{\Delta H}, \quad (2)$$

where H_{max} is the maximum applied dc magnetic field to saturate the impedance of the ribbon. ΔH is a measure of the full width at half maximum (FWHM). These two parameters are the main figures of merit that we monitor for the series of samples measured and on which the analysis of the sensor response can be determined.

3. Results and discussion

Fig. 2 shows the XRD pattern of the $Co_{69}Fe_{4.5}Ni_{1.5}Si_{10}B_{15}$ as-quenched ribbon. It is clear that the pattern exhibited only one broad peak around $2\theta = 45^\circ$, which is often known as a diffuse halo, indicating that the sample prepared is nearly amorphous in nature.

Fig. 3 shows the AFM images of the surface topography of the $Co_{69}Fe_{4.5}Ni_{1.5}Si_{10}B_{15}$ amorphous ribbon sample for both surfaces. Herewith the free surface of the ribbon was that had no contact with the surface of the copper wheel (see the upper panel of Fig. 3) and the wheel-side ribbon surface was that had direct contact with the surface of the copper wheel (see the lower panel of Fig. 3). The AFM image indicates the distribution of protrusions with very high and uniform density for the free surface of the ribbon, unlike in the case of the wheel-side surface of the ribbon. The root mean squared (rms) surface roughness ($R_q = (1/n^2)\sqrt{\sum_{i=1}^{n} z_i^2}$, where z

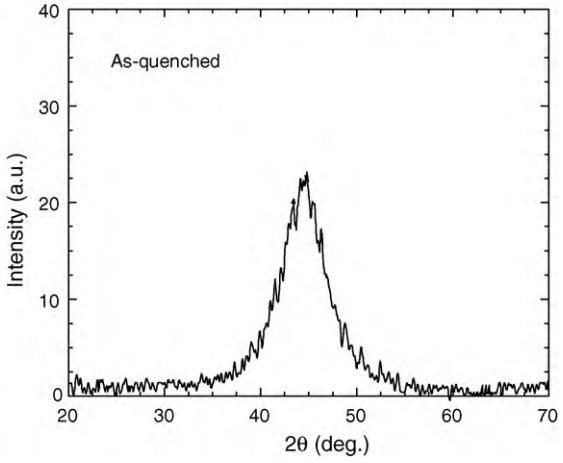

Fig. 2. The XRD pattern of the $Co_{69}Fe_{4.5}Ni_{1.5}Si_{10}B_{15}$ as-quenched amorphous ribbon.

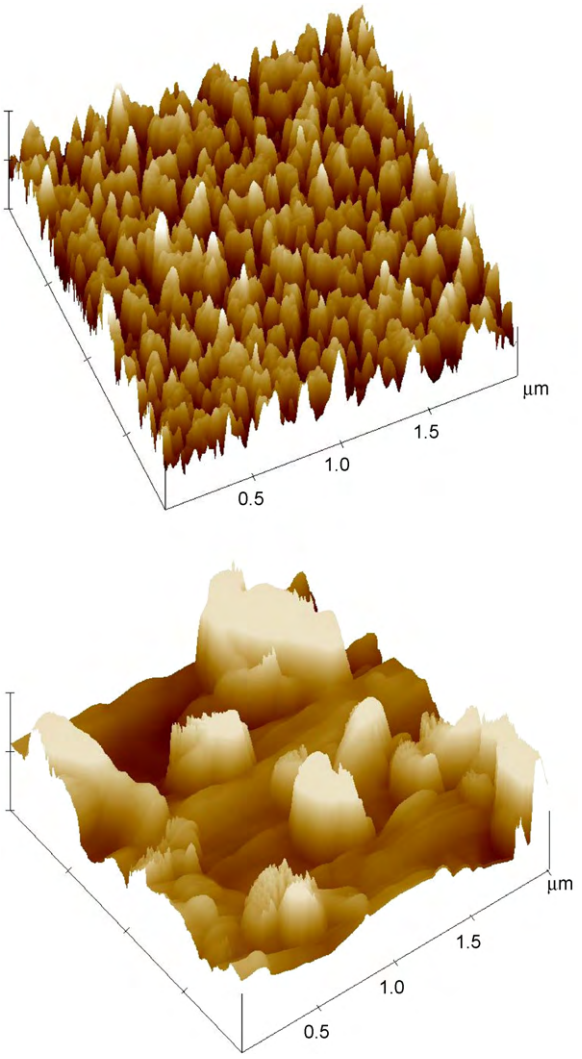

Fig. 3. The AFM images of the $Co_{69}Fe_{4.5}Ni_{1.5}Si_{10}B_{15}$ amorphous ribbon sample for the free surface (upper panel) and for the wheel-side surface (lower panel).

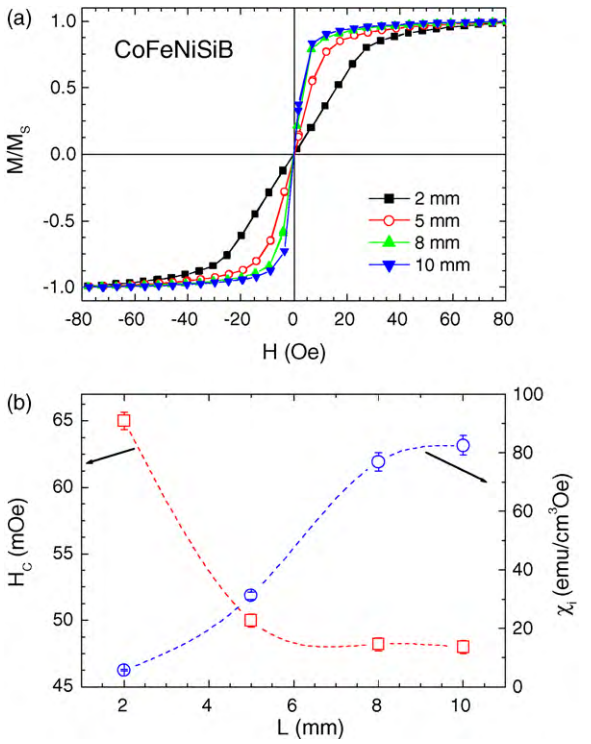

Fig. 4. (a) Magnetic hysteresis loops of $Co_{69}Fe_{4.5}Ni_{1.5}Si_{10}B_{15}$ amorphous ribbons with different lengths $L = 2$, 5, 8, and 10 mm; and (b) sample length dependences of coercivity (H_c) and initial susceptibility (χ_i).

is the average amplitude of the topographical feature) was determined from the corresponding topographical data of Fig. 3 to be about 2.153 and 80.518 nm for the free surface of the ribbon and for the wheel-side surface of the ribbon, respectively.

Fig. 4(a) shows M–H loops taken at room temperature for $Co_{69}Fe_{4.5}Ni_{1.5}Si_{10}B_{15}$ amorphous ribbons with different lengths ($L = 2$, 5, 8 and 10 mm). The coercivity (H_c) and initial susceptibility (χ_i) extracted from these curves are plotted against sample length (L) as shown in Fig. 4(b). It can be observed that H_c increases and χ_i decreases as L decreases from 10 to 2 mm. It is worth noting that χ_i starts to decrease strongly for samples with $L < 8$ mm. This may be reconciled with the fact that the soft magnetic properties are lost when the sample length becomes less than a critical length ($L_0 \sim 8$ mm), and the demagnetization effect becomes significant for the ribbons with $L < L_0$ [18]. Accordingly, it seems to suggest that due to the strong demagnetization effect, closure domains could be formed in the ends of the $Co_{69}Fe_{4.5}Ni_{1.5}Si_{10}B_{15}$ ribbons which largely modified the original transverse domain structure thus reducing χ_i. Meanwhile, domain wall pinning likely promoted magnetic hardness in the ends of these ribbons which consequently resulted in an increase of H_c. The presence of residual stresses or defects created during sample processing and their influence on the domain structure as the ribbon length varied could also contribute to the variation of H_c. The non-saturation of magnetization observed for the ribbons with $L < L_0$ (Fig. 4(a)) is indicative of the formed closure domain structure. A similar behavior was also observed for the case of Fe-based nanocrystalline wires by Vazquez et al. [11]. However, we recall that no evidence of the existence of L_0 was found in that work because the length of all measured samples was less than the critical length [11].

Fig. 5 shows the magnetic field dependence of GMI ratio ($\Delta Z/Z$) at two representative frequencies, $f = 1$ and 6 MHz, for $Co_{69}Fe_{4.5}Ni_{1.5}Si_{10}B_{15}$ amorphous ribbons with different lengths ($L = 2$, 5, 8 and 10 mm). It can be observed that for the case at 1 MHz, $\Delta Z/Z$ reaches the largest value for the $L = 2$ mm sample, while for the 6 MHz case, the largest $\Delta Z/Z$ is achieved for the $L = 8$ mm sample. To better illustrate this feature, we display in Fig. 6(a) the frequency dependence of maximum GMI ratio ($[\Delta Z/Z]_{max}$) for all samples investigated. As one can see clearly from this figure, at $f < 3$ MHz the $L = 2$ mm sample shows the largest value of $[\Delta Z/Z]_{max}$, whereas at $f > 3$ MHz the largest $[\Delta Z/Z]_{max}$ is achieved for the $L = 8$ mm sample. A general trend observed for all the samples is that with increasing frequency in the range of 0.1–10 MHz, $[\Delta Z/Z]_{max}$ first increases, reaches a maximum at a critical frequency (f_0), and then decreases for higher frequencies. This trend can be interpreted by considering the relative contributions of domain wall motion and magnetization rotation to the transverse permeability and hence the GMI effect [20]. At low frequencies below 1 MHz, $[\Delta Z/Z]_{max}$ is relatively low due to the contribution of the induced magneto-inductive voltage to the measured magnetoimpedance [2]. In the range 1 MHz $\leq f \leq f_0$ MHz, the skin effect is dominant, hence a higher $[\Delta Z/Z]_{max}$ is observed. Above f_0, $[\Delta Z/Z]_{max}$ decreases with increasing frequency. This is because, in this frequency region, the domain wall displacements are strongly damped owing to eddy currents thus contributing less to the transverse permeability and hence $[\Delta Z/Z]_{max}$.

It has been shown that the surface roughness of the sample becomes important at high frequency, where the skin effect is strong [1,20]. This is not only because the skin depth may

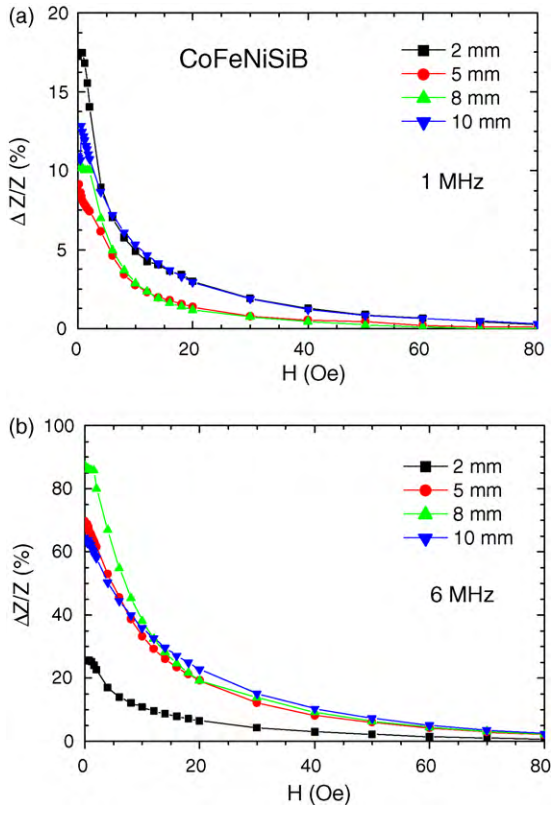

Fig. 5. Magnetic field dependence of GMI ratio ($\Delta Z/Z$) at 1 MHz (a) and 6 MHz (b) for $Co_{69}Fe_{4.5}Ni_{1.5}Si_{10}B_{15}$ amorphous ribbons with different lengths L = 2, 5, 8, and 10 mm.

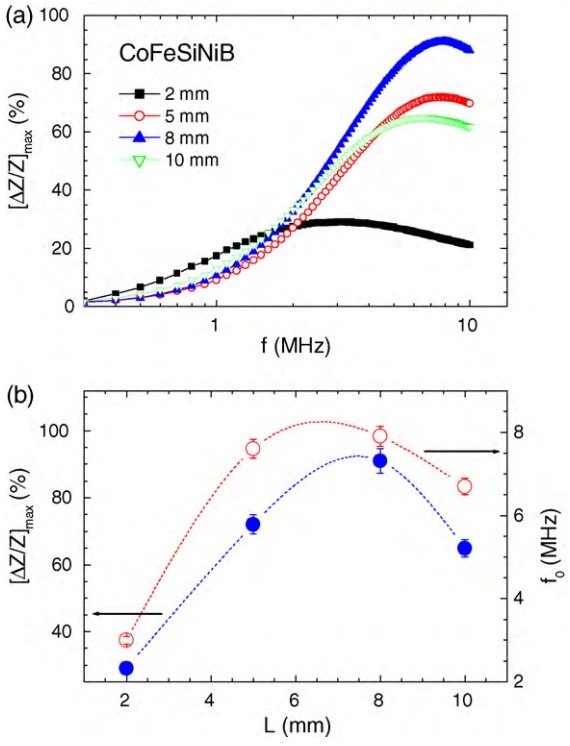

Fig. 6. (a) Frequency dependence of maximum GMI ratio ($[\Delta Z/Z]_{max}$) and (b) sample length dependences of $[\Delta Z/Z]_{max}$ and critical frequency (f_0).

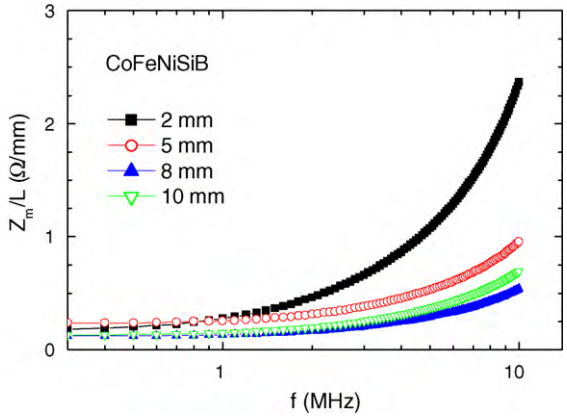

Fig. 7. Frequency dependence of the reduced impedance (Z_m/L) for $Co_{69}Fe_{4.5}Ni_{1.5}Si_{10}B_{15}$ amorphous ribbons with different lengths L = 2, 5, 8, and 10 mm.

become smaller than the surface irregularities, but also due to stray fields, which appear on the rough surface and cause a considerable reduction in the GMI magnitude [20–24]. To check if the surface roughness plays a role in the high frequency GMI behavior in the $Co_{69}Fe_{4.5}Ni_{1.5}Si_{10}B_{15}$ amorphous ribbons, we have calculated the skin depth (δ_m) of the samples at the highest measured frequency of 10 MHz using a simple relationship given by Kuzminski and Lachowicz [25]:

$$\delta_m = \frac{a}{2}\frac{R_{dc}}{R_{ac}}, \tag{3}$$

where a is the ribbon thickness, R_{dc} is the dc resistance and R_{ac} is the ac resistance at a given frequency of the ac current (in our case, the value of R_{ac} was taken at f = 10 MHz). The calculated values of δ_m are 3.98, 3.06, 2.83, and 2.25 μm for the samples with L = 2, 5, 8, and 10 mm, respectively. These values are much larger than the rms surface roughness of the ribbon determined from AFM ($R_q \sim 2.153$ nm = 2.153×10^{-3} μm for the free surface of the ribbon and $R_q \sim 80.518$ nm = 8.0518×10^{-2} μm for the wheel-side surface of the ribbon). Therefore, the surface roughness does not play a significant role in the GMI behavior in the present samples, at least in the investigated frequency range of 0.1–10 MHz.

Fig. 6(b) shows the sample length (L) dependence of $[\Delta Z/Z]_{max}$ and f_0. It can be observed that when the sample length increases from 2 to 10 mm, $[\Delta Z/Z]_{max}$ and f_0 first increase, reach the maximum values at L = 8 mm, and then decrease for longer L. This clearly indicates that there exists a critical length ($L_0 \sim \cong 8$ mm) for the case of $Co_{69}Fe_{4.5}Ni_{1.5}Si_{10}B_{15}$ amorphous ribbons. The existence of L_0 is further confirmed by considering the frequency dependence of the reduced impedance (Z_m/L) in Fig. 7. It can be seen that for samples with $L < L_0 \sim 8$ mm the magnitude of Z_m/L increases with decreasing L, indicating the importance of the demagnetization effect and the possible formation of closure domains in these samples [11]. This is in full agreement with the strong reduction of initial susceptibility (χ_i) seen in Fig. 4 for samples with $L < L_0 \sim 8$ mm. For samples with $L > L_0$, however, the magnitude of Z_m/L decreases with decreasing L, which arises mainly from the decrease of electrical resistance of the ribbon [17].

From a sensor application perspective, it is essential to understand the influence of sample length on the field sensitivity of GMI (η). We have calculated η from the GMI profiles using Eq. (2). Fig. 8(a) displays the frequency dependence of η for the samples with different L. The maximum value of η and f_0 (the frequency at which η reaches the largest value) deduced from Fig. 8(a) are plotted against L as shown in Fig. 8(b). Like the case reported in Fig. 6, both η and f_0 first increase with increasing L, reach the maximum values at L = 8 mm, and then decrease for longer L. This

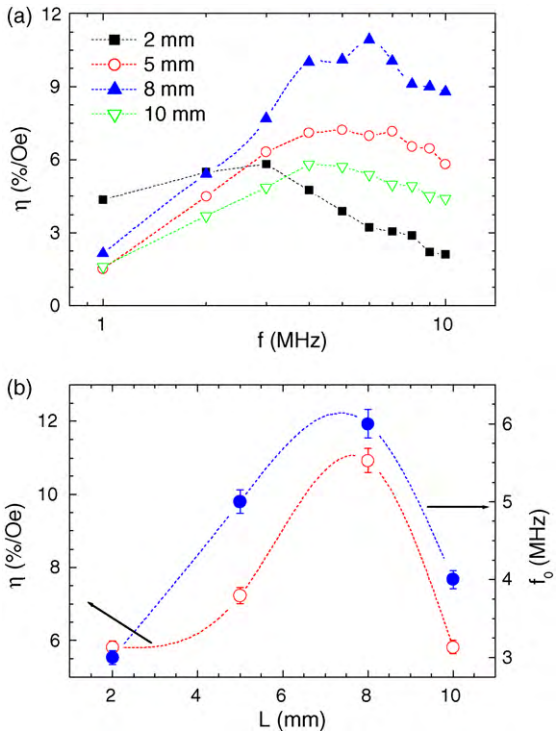

Fig. 8. (a) Frequency dependence of magnetic response (η) and (b) sample length dependences of maximum magnetic response (η_{max}) and critical frequency (f_0).

once again confirms the existence of the critical length ($L_0 \sim 8$ mm) for the $Co_{69}Fe_{4.5}Ni_{1.5}Si_{10}B_{15}$ amorphous ribbons. Thus an important feature that emerges for the first time from our study is that we demonstrate the existence of a critical length (L_0) in a magnetic ribbon. We show that when $L = L_0$, the GMI effect and η reach the largest values at the highest critical frequency (f_0). The GMI effect and η decrease for the cases $L > L_0$ and $L < L_0$. This finding provides a clear understanding of the effect of critical length and provides guidance for possible optimization of material dimensions and geometry employed in GMI-based magnetic sensors.

The origin of L_0 in the $Co_{69}Fe_{4.5}Ni_{1.5}Si_{10}B_{15}$ amorphous ribbons can be explained on the basis of the skin effect model [2]. According to this model, a larger GMI effect is achieved in magnetic ribbons with larger transverse susceptibility (μ_T) and smaller electrical resistance (R_{dc}). We note that both μ_T and R_{dc} depend on the length of the ribbon, L [5–8,17]. While R_{dc} decreases gradually with decreasing L ($R_{dc} = 1.8$, 1.46, 1.02, 0.69 Ω for $L = 10$, 8, 5, 2 mm, respectively), μ_T is almost independent of L for $L > L_0$ but is strongly reduced for $L < L_0$ caused by the demagnetization effect. Since the contributions of μ_T and R_{dc} to GMI are opposite, one can expect the existence of a critical length (L_0) at which the largest value of GMI effect is achieved. For samples with $L > L_0$, the decrease of L reduces R_{dc} which dominantly contributes to an increase of GMI effect. This explains the increase of GMI effect in Co-based microwires with L decreasing from 4 to 1 mm [17]. For samples with $L < L_0$, the decrease of GMI results mainly from the strong decrease of μ_T due to the demagnetization effect. This explains why the GMI effect decreased with decreasing L in Co-based amorphous ribbons [12–14], Fe-based nanocrystalline ribbons [15,16] and CoSiB/Cu/CoSiB layered thin films [5]. Actually, the magnitude of L_0 depends on the type of domain structure [11,17,18], and it has been found that the critical length is shorter for Co-based wires than for Fe-based wires [18]. A final note is that while the observed GMI effect largely varied with changing L for the case of magnetic wires and ribbons [11–16], it was almost independent of L for the case of a $La_{0.7}Sr_{0.3}MnO_3$ manganite [26]. This could arise from the fact that the demagnetization effect played less important role in the bulk and thick manganite sample [26].

4. Conclusions

The influence of sample length ($L = 2$, 5, 8, and 10 mm) on the GMI effect and its field sensitivity (η) in $Co_{69}Fe_{4.5}Ni_{1.5}Si_{10}B_{15}$ amorphous ribbons has been studied. We reveal the existence of a critical length ($L_0 \sim 8$ mm) in the $Co_{69}Fe_{4.5}Ni_{1.5}Si_{10}B_{15}$ amorphous ribbons. The largest GMI effect and η are achieved for samples with $L = L_0$. For samples with $L < L_0$, the GMI effect and η decrease with decreasing L, resulting from the possible formation of closure domain structures near the ends of the sample due to the demagnetization effect. For samples with $L > L_0$, the increase of GMI effect and η with decreasing L can be attributed to the decrease of electrical resistivity. The critical frequency (f_0), at which the maximum GMI and η are achieved, reaches the largest value for samples with $L = L_0$ and shifts to lower values for samples with $L < L_0$ and $L > L_0$. Our studies provide physical insights into the effect of critical length and give useful insights based on geometry considerations for optimization of GMI effect in sensitive GMI-based magnetic sensors.

Acknowledgements

The authors acknowledge support from USAMRMC through grant number W81XWH-07-1-0708 and the NSF through GOALI grant CMMI-0728073. A.T. Le would like to acknowledge the support from the National Foundation for Science and Technology Development (NAFOSTED) through Grant number 103.02.96.09.

References

[1] M.H. Phan, H.X. Peng, Prog. Mater. Sci. 53 (2008) 323.
[2] L.V. Panina, K. Mohri, Appl. Phys. Lett. 65 (1994) 1189.
[3] H.Q. Guo, H. Kronmuller, T. Dragon, Z.H. Cheng, B.G. Shen, J. Appl. Phys. 89 (2001) 514.
[4] R.L. Sommer, C.L. Chien, Appl. Phys. Lett. 67 (1995) 3346.
[5] T. Morikawa, Y. Nishibe, H. Yamadera, IEEE Trans. Magn. 33 (1997) 4367.
[6] J. Hu, H. Qin, F. Zhang, R.K. Zheng, J. Appl. Phys. 91 (2002) 7418.
[7] A.T. Le, M.H. Phan, C.O. Kim, M. Vaquez, H. Lee, N.Q. Hoa, S.C. Yu, J. Phys. D Appl. Phys. 40 (2007) 4582.
[8] J.M. Barandiaran, A. Garcia-Arribias, J.L. Munoz, G.V. Kurlyandskaya, IEEE Trans. Magn. 38 (2002) 3051.
[9] V. Zhukova, A. Chizhik, A. Zhukov, A. Torcunov, V. Larin, J. Gonzalez, IEEE Trans. Magn. 38 (2002) 3090.
[10] A. Zhukov, M. Ipatov, J. Gonzalez, J.M. Blanco, V. Zhukova, J. Magn. Magn. Mater. 321 (2009) 822.
[11] M. Vazquez, Y.F. Li, D.X. Chen, J. Appl. Phys. 91 (2002) 6539.
[12] K.C. Mendes, F.L.A. Machado, J. Magn. Magn. Mater. 177–181 (1998) 111.
[13] G.V. Kurlyandskaya, J.M. Barandiarán, M. Vázquez, D. García, N.V. Dmitrieva, J. Magn. Magn. Mater. 215–216 (2000) 740.
[14] V.S.N. Murthy, S. Venkatesh, G. Markandeyulu, J. Appl. Phys. 99 (2006) 08F108.
[15] K. An, J. Hu, H. Qin, T. Han, Y. Wang, X. Yu, B. Li, Rare Mater. 23 (2004) 235.
[16] H. Qin, X. Yu, B. Li, Y. Hao, S. Huang, J. Hu, M. Jiang, Mater. Trans. 46 (2005) 1261.
[17] M.H. Phan, H.X. Peng, S.C. Yu, M.R. Wisnom, J. Magn. Magn. Mater. 316 (2007) e253.
[18] V. Zhukova, N.A. Usov, A. Zhukov, J. Gonzalez, Phys. Rev. B 65 (2002) 134407.
[19] K.S. Byon, S.C. Yu, C.G. Kim, J. Appl. Phys. 89 (2001) 7218.
[20] M.H. Phan, H.X. Peng, M.R. Wisnom, S.C. Yu, J. Appl. Phys. 98 (2005) 014316.
[21] L. Kraus, Sen. Actuator A 106 (2003) 187.
[22] F. Amalou, M.A.M. Gijs, J. Appl. Phys. 90 (2001) 3466.
[23] A.T. Le, C.O. Kim, N. Chau, N.D. Cuong, N.D. Tho, N.Q. Hoa, H.B. Lee, J. Magn. Magn. Mater. 307 (2006) 178.
[24] X.P. Li, Z.J. Zhao, H.L. Seet, W.M. Heng, T.B. Oh, J.Y. Lee, J. Appl. Phys. 94 (2003) 6655.
[25] M. Kuzminski, H.K. Lachowicz, J. Magn. Magn. Mater. 267 (2003) 35.
[26] A. Rebello, R. Mahendiran, Appl. Phys. Lett. 96 (2010) 032502.